M a t h e m a t i c a
B a l k a n i c a

New Series Vol. 26, 2012, Fasc. 3–4

Numerical Simulations of Absorbing Boundary Conditions

Vasko Kokalanov[1], *Vlatko Sesov*[2]

Presented at MASSEE International Conference on Mathematics MICOM-2009

Several analysis to show the advantages of the absorbing boundaries compared to the classical Dirichlet and Neumann boundaries are performed. Some precautions of the weaknesses of the model which are identified during the analysis are also given. The conditions and several recommendations for optimal work of the model are presented as well.

MSC 2010: 35Q86
Key Words: absorbing boundaries, Dirichlet and Neumann boundaries

1. Introduction

Problems like dynamic behavior of infinite domains are solvable only if they are limited to finite computational domain. With the use of the assumption that the whole energy is produced from sources circumscribed in this limited domain and that there are no energy sources at very large distances from the region which is analyzed, a finite domain can be isolated. This truncation will be made with introducing of the domain's artificial boundaries. Using the finite difference method, a half- and full-space are transformed in numerical model. It consist two parts: inner part, where an explosive source (Gaussian pulse) excites wave motion and outer part – the boundaries of the model which absorb the energy from the inner part.

2. Mathematical model

Geometry – The 2-D model is vertical section of homogenous and isotropic ground layer (figure 1). It presents a rectangular grid with uniform distributed points in both directions ($\Delta h = 2m$). The ground characteristics

are defined indirectly (eq. 2) by the shear v_s and the compressional velocities v_p. At point S an explosive source is applied.

Equation of motion. Two coupled, second-order, partial differential equation are used to be described the motion of the P-waves and vertically polarized shear SV- waves [5]:

$$\rho\frac{\delta^2 u}{\delta t^2} = (\lambda+2\mu)(\frac{\delta^2 u}{\delta x^2}+\frac{\delta^2 w}{\delta x\delta z})+\mu(\frac{\delta^2 u}{\delta z^2}-\frac{\delta^2 w}{\delta x\delta z})$$

$$\rho\frac{\delta^2 w}{\delta t^2} = (\lambda+2\mu)(\frac{\delta^2 u}{\delta x\delta z}+\frac{\delta^2 w}{\delta z^2})+\mu(\frac{\delta^2 w}{\delta x^2}-\frac{\delta^2 u}{\delta x\delta z})$$

where u and w are the horizontal and the vertical displacement respectively, ρ is the density of the medium, t is the time, while λ and μ are the Lame parameters. The two velocities, v_p and v_s, are dependent on the ground characteristics:

$$v_p = \sqrt{\frac{\lambda+\mu}{\rho}};\ v_s = \sqrt{\frac{\mu}{\rho}} \qquad (2)$$

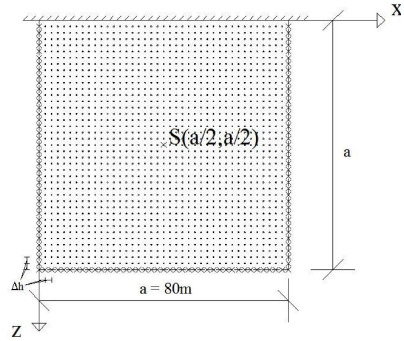

Figure 1: Geometry

The horizontally polarized SH-waves are uncoupled with P- and SV-waves and hence are not included in the analysis.

Initial conditions. At time $t = 0$ there is no motion, thus $u = w = 0$. Since the numerical model is explicit, the displacements at time $t = 1$ are prescribed only at the source point.

Boundary conditions. In order to have half space model, at level $z = 0$, a free surface boundary conditions are prescribed. That means that the stresses must vanish on this boundary:

$$(\alpha^2-2\beta^2)\frac{\delta u}{\delta x}+\alpha^2\frac{\delta w}{\delta z}=0;\quad \frac{\delta u}{\delta z}+\frac{\delta w}{\delta x}=0 \qquad (3)$$

The other three implemented boundary conditions are based on paraxial approximations [2]. In [1] are given the two paraxial approximations which are used in this analysis:

$$A1: u_z + B_1 u_t = 0;\quad A2: u_{tz} + C_1 u_{tt} + C_2 u_{tx} + C_3 u_{tx} = 0 \qquad (4)$$

Source excitations. The Gaussian pulse which describes the source is:

$$f(t) = e^{-\alpha(t-t_0)^2} \tag{5}$$

where α (here $\alpha = 3000$) controls the wave length content of excitation, t is the actual time of calculation and t_0 (here $t_0 = 0.036$) is time when the function hits its maximum.

3. Numerical model

Equation of motion. In [5] are given the finite-difference numerical approximations which are used to simulate the wave propagation in all grid points:

$$\begin{aligned} u(m,n,i+1) = {} & 2u(m,n,i) - u(m,n,i-1) + F^2[u(m+1,n,i)- \\ & - 2u(m,n,i) + u(m-1,n,i)] + F^2(1-\gamma^2)[w(m+1,n+1,i)- \\ & - w(m+1,n-1,i) - w(m-1,n+1,i) + w(m-1,n-1,i)]+ \\ & + F^2\gamma^2[u(m,n+1,i) - 2u(m,n,i) + u(m,n-1,i)] \end{aligned} \tag{6}$$

$$\begin{aligned} w(m,n,i+1) = {} & 2w(m,n,i) - w(m,n,i-1) + F^2[w(m,n+1,i)- \\ & - 2w(m,n,i) + w(m,n-1,i)] + F^2(1-\gamma^2)[u(m+1,n+1,i)- \\ & - u(m+1,n-1,i) - u(m-1,n+1,i) + u(m-1,n-1,i)]+ \\ & + F^2\gamma^2[w(m+1,n,i) - 2w(m,n,i) + w(m-1,n,i)] \end{aligned}$$

where $x = mh$, $z = nh$ and $t = i\Delta t$. Δt is the time step and h is the grid interval in both x- and z-directions. Furthermore $\gamma = v_s/v_p$, where v_s and v_p are the velocities (eq. 2). The parameter F can be calculated by: $F = v_p\Delta t/h$.

Boundary conditions

Absorbing boundary conditions. In [1] and [3] are proposed the following formulation of finite difference scheme for the second-order elastic boundary conditions:

Bottom

$$\begin{aligned} 0 = {} & D_-^z D_0^t u(m,a,i) + \frac{1}{2}C_1 D_+^t D_-^t (u(m,A,i) + u(m,a-1,i))+ \\ & + \frac{1}{2}C_2 D_+^t D_0^x (u(m,a,i-1) + u(m,a-1,i)) + \frac{1}{2}C_3 D_+^x D_-^x (u(m,a,i-1)+ \\ & + u(m,a-1,i+1)) \end{aligned}$$

Left side

$$0 = D^x_+ D^t_0 u(0,n,i) - \frac{1}{2} C'_1 D^t_+ D^t_- (u(0,n,i) + u(1,n,i)) + \\ + \frac{1}{2} C_2^T D^t_+ D^z_0 (u(0,n,i-1) + u(1,n,i)) - \frac{1}{2} C'_3 D^z_+ D^z_- (u(0,n,i-1) + \\ + u(1,n,i+1))$$

Right side

$$0 = D^x_- D^t_0 u(a,n,i) + \frac{1}{2} C'_1 D^t_+ D^t_- (u(a,n,i) + u(a-1,n,i)) + \\ + \frac{1}{2} C_2^T D^t_+ D^z_0 (u(a,n,i-1) + u(a-1,n,i)) + \frac{1}{2} C'_3 D^z_+ D^z_- (u(a,n,i-1) + \\ + u(a-1,n,i+1)) \tag{7}$$

D^z_-, D^z_+ and D^z_0 are the backward, forward and central differential operators with respect to the variable z.

According to [3] the two new matrices C'_1 and C'_3 are:

$$C'_1 = \begin{bmatrix} \frac{1}{v_p} & 0 \\ 0 & \frac{1}{v_s} \end{bmatrix}; \quad C'_3 = \frac{1}{2} \begin{bmatrix} v_p - 2v_s & 0 \\ 0 & v_s - 2v_p \end{bmatrix}$$

and C_2^T is the transposed matrix of C_2. For the corner points and for their first neighboring points on the boundaries, rotated formulation of A1 is used:
Bottom-right corner:

$$u_z + u_x + M_{ut} = 0$$

$$(D^z_- + D^x_- + M(v_p, v_s), D^t_-) u(m,n,i) = 0$$

Bottom-left corner:

$$(D^z_- - D^x_+ + M(v_s, v_p), D^t_-) u(m,n,i) = 0$$

and the newly introduced matrix M is

$$M(v_s, v_p) = \frac{1}{\sqrt{2}} \begin{bmatrix} \frac{1}{v_s} + \frac{1}{v_p} & \frac{1}{v_s} - \frac{1}{v_p} \\ \frac{1}{v_s} - \frac{1}{v_p} & \frac{1}{v_s} + \frac{1}{v_p} \end{bmatrix}$$

Free surface. The upper border is free surface. Because the points could not be solved only by the elastic wave equation, additionally new pseudonodes should be introduced. Since the free surface boundary has coordinate $z = 0$, the pseudonodes will have index -1 (figure 2). The unknown displacement for

these nodes will be calculated by the stress free conditions (eq. 3). The finite difference code for (3) is:

$$\begin{aligned} u(x,-1,t) &= u(x,0,t) + 0,5[w(x+1,0,t) - w(x-1,0,t)] \\ w(x,-1,t) &= w(x,0,t) + 0,5(1-\gamma^2)[u(x+1,0,t) - u(x-1,0,t)] \end{aligned} \quad (8)$$

Remark: Equations (8) have this form only if grid size is $dx = dz = h$.

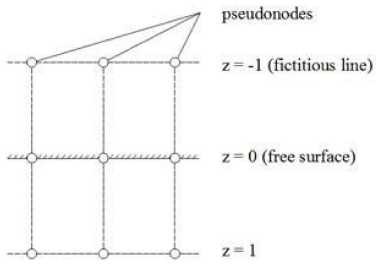

Figure 2: Free surface

For the upper corner points, where the intersection is between the vertical absorbing boundaries and the fictitious line, the displacements are calculated using the first-order boundary conditions according to [3]:

$$\begin{aligned} (D_+^x - C'_1 D_+^t)u(0,-1,t) &= 0 \\ (D_-^x + C'_1 D_+^t)u(a,-1,t) &= 0 \end{aligned} \quad (9)$$

Source. The term which represents the source in the equation of motion inherits the following expression $\delta(r - r_0)f(t)$. It is easy to recognize the Dirac delta function which has value infinity when $r = r_0$. That means that at the point where the force is applied, the stresses are going to infinity. To avoid this, the source is applied in four surrounding points with the same function in time (eq. 5) producing radial displacements equal in all directions.

Stability conditions

Grid mesh. A physically meaningful calculations requires that the finite difference algorithm should be stable, i.e., the difference between the exact and the numerical solutions of a finite difference equation must remain bounded as the time index i increases, Δt remaining fixed for all m and n. The authors in [4] have shown that the system of equations (6) is stable provided that:

$$F = \frac{\alpha v_p}{h} \leq (1 + \frac{\alpha^2}{\beta^2})^{-1/2}; \quad \Delta t \leq \frac{h}{(1 + \frac{\alpha^2}{\beta^2})^{1/2}} \quad (10)$$

which shows that the time increment must obey a constraint imposed by the choice of a grid interval h as well as the values of the P- and SV-wave velocities in particular homogeneous layer [5].

Absorbing boundaries. The stability of the absorbing boundaries is referred to the ratio of the SV- and P-wave velocities β/α. Experimenting with this ratio,

the authors of [4] proved that the instability appears when the ratio is smaller than 0.46.

Beside the instability due to the ratio, the borders can derive a finite difference solution into instability due to inappropriately defined free surface boundary conditions.

4. Numerical example

The first test was performed on a model with four reflecting boundaries (here Dirichlet boundary conditions $u = w = 0$) and velocities $v_s = 250$ and $v_p = \sqrt[3]{250}$. Figure 3 clearly shows that the waves exited from the source are reflected back in the model and hence the whole energy is occupied between the borders.

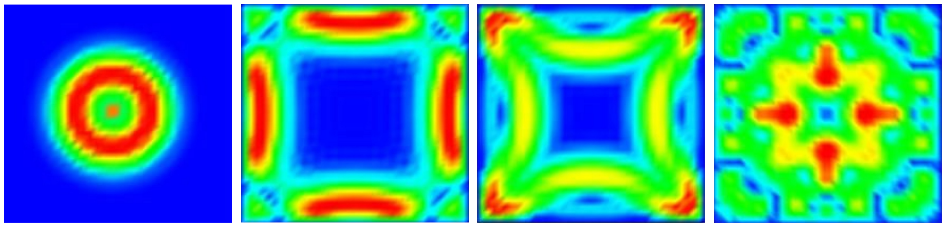

Figure 3: Dirichlet boundaries

Opposite to that, the graphical output of the radial displacements in time (figure 4), obtained with the model which has free surface on top and three absorbing boundaries, are showing that through the absorbing boundaries the waves can dispersed the energy outside of the model. The reflection from the upper surface shows that Neuman boundary conditions are producing reflections. Also this reflected wave filed will exit the model through the absorbing boundaries.

Although the absorbing boundaries make absorption of energy, they are defined as approximations and thus they must produce some reflection. The reflection is dependent on the order of the paraxial approximation and the angle of incidence. The higher is the order of the paraxial approximation the higher is the exactness. The numerical test of the model proved those results. On figure 5 one can see the different reflection at the same boundary, but at different points.

The first point (1,39) is neighbor point to the bottom-left corner, which is prescribed as rotated A1. The second point (20,39) is the point above the middle of the bottom boundary, which is prescribed by A2. The peaks which are next to the wave field peak are tailing peaks and are result of the reflections and

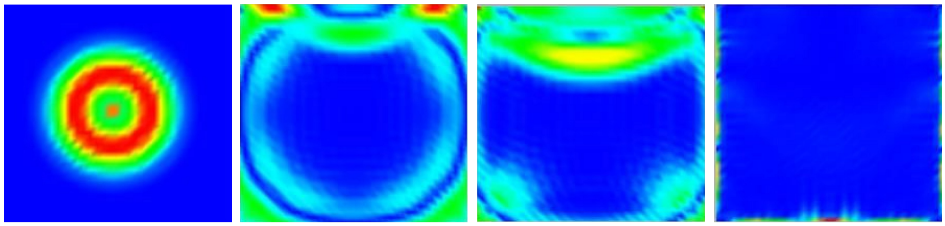

(a) t = 0.06 s (b) t = 0.14 s (c) t = 0.16 s (d) t = 0.16 s

Figure 4: Absorbing boundaries and free surface

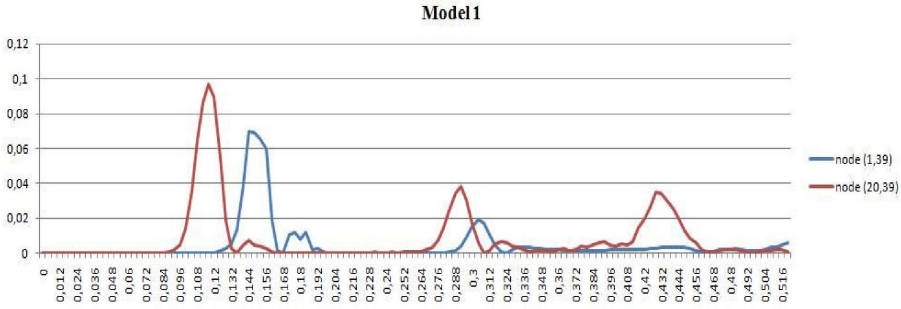

Figure 5: Reflection and grid dispersion

grid dispersion. The tailing peak at node (1,39) (the blue line) is much bigger than the same peak at node (20,39) (red line) which confirms that the order of the paraxial approximations makes A1 to induce greater reflections than A2.

Despite the order of the approximation, big influence of the reflection has also the angle of incidence. The point (1,39) is located near the corner where the angle is about 45^0. The angle at the location of the point (20,39) is 0^0. As the given results in [1], figure 5 confirms that the absorbing boundaries produce more reflection at the point where the angle of incidence is bigger.

The biggest disadvantage of these boundary conditions is the corner formulation. In [1] is given an improvement by introducing the A1 approximation at the corners. But this is only valid when two absorbing boundaries are intersecting. In the top-left and the top-right corners the intersection is between the free surface and the absorbing boundary and thus A1 is not an option. These corners are uncovering the greatest weakness of the model. They produce in-

stability which have influence at the rest points. Calling back Figure 5 one can see that the displacements for node (20,39) have three peaks. The first one is from the wave field coming from the source, the second one is from the wave field which is reflected from the free surface and the last one is result of the instability at the top-left and top-right corners.

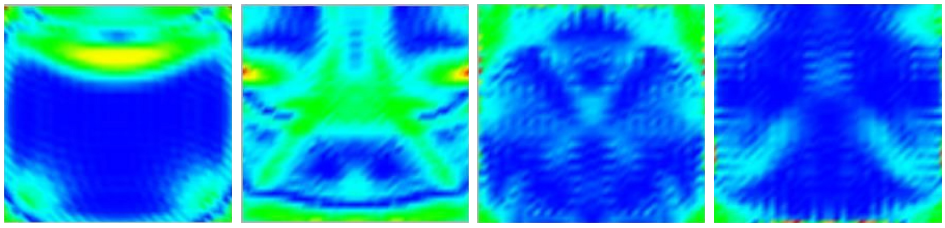

Figure 6: Numerical instability

On picture a) (figure 6) there are extremes colored with red exactly at those corners. On b) these extreme values are moving downwards and in the last two pictures can be seen that these extremes influence the displacements on the bottom boundary as well. These extremes are leaving the model but meanwhile new one are produced. This leads to instability of the boundaries in time. It would be no problem if the instability is happening only on the boundaries. But because of the interaction between the grid mesh and the absorbing boundaries, the increment is transferred in the inner part of the model. The displacement in time for node (20,40) are show on the next figure:

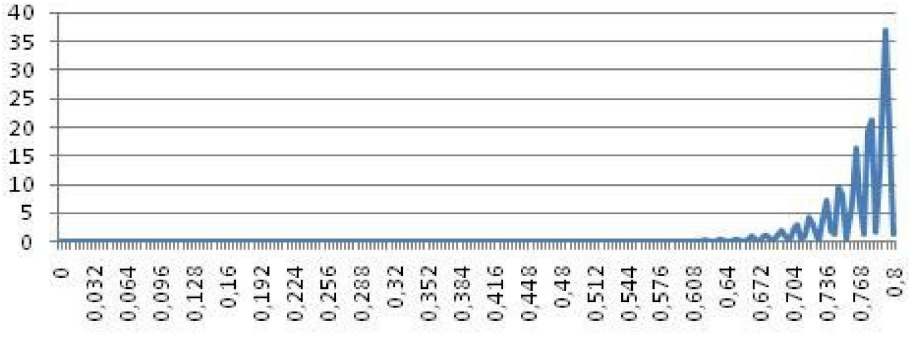

Figure 7: Displacements in time

Numerically stable model requires stable inner part as well. One important point is dimensions of the model regarding to the velocity of the waves. Wavelength is proportional to the wave velocity. Hence increasing the velocity means that the model should be increased such it captures the full wavelength. The dimensions of the model must be careful defined it would represent the full wave field and it's propagation through the medium. Figure 8 demonstrates this kind of instability.

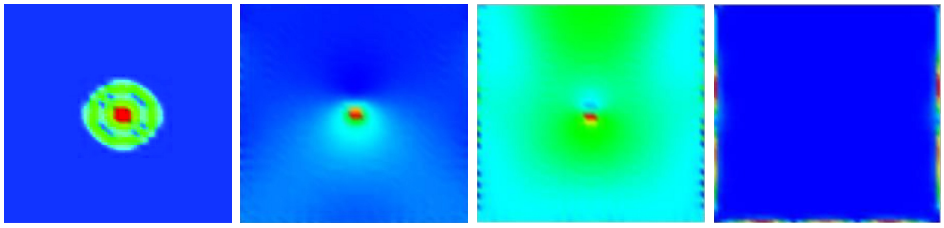

Figure 8: Inappropriate grid mesh

Another important issue for numerical stability is the distance between the grid points. The investigations from the past are suggesting that the number of grid points per wavelength at the upper half-power frequency of the source should be approximately ten or more in order to satisfy limit grid dispersion (figure 9).

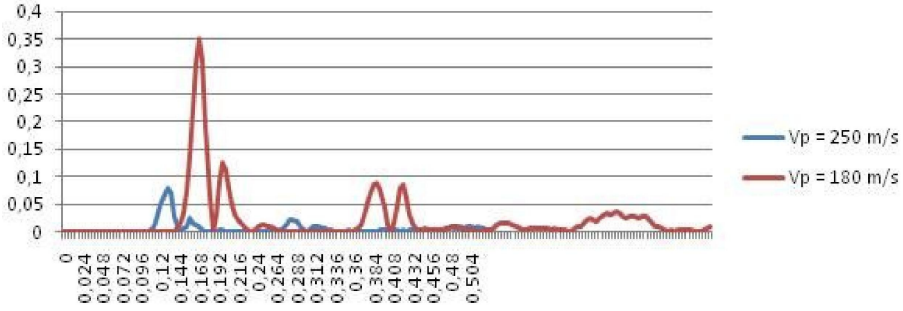

Figure 9: Grid dispersion

By decreasing the velocity, the wavelength is decreased too. For same grid mesh less grid points are used per wavelength and hence the grid dispersion ("tailing" peak) is bigger.

References

[1] R. Clayton, B. Engquist. Absorbing Boundary Conditions for Acoustic and Elastic Waves Equations. // *BSSA*, **67**, No.6, 1977, 1529–1549.

[2] R. Clayton, A. Majda. Absorbing boundary conditions for the Numerical Solution of Waves. // *Math. Comput.* **31**, 1977, 629–651.

[3] M. Fuyuki, Y. Matsumoto. Finite Difference Analysis of Rayleigh Wave Scattering at a Trench. // *BSSA*, **70**, 1980, 2051–2069.

[4] S. H. Emerman, R. A. Stephen. Comment on "Absorbing Boundary Conditions for Acoustic and Elastic Waves Equations" by R. Clayton and B. Engquist. // *BSSA*, **73**, No.6, 1983, 661–665;

[5] K. R. Kelly, R. W. Ward, S. Treitel , M. Alford. Synthetic Seismogram: a finite difference approach. // *Geophysics*, **41**, 2–21.

[1] *Department of Computer Science*
University "Goce Delcev"
Stip
R. MACEDONIA
E-MAIL: vasko.kokalanov@ugd.edu.mk

[2] *Institute of Earthquake Engineering*
and Engineering Seismology
Skopje
R. MACEDONIA

Received 15.01.2010